Available online at www.sciencedirect.com
ScienceDirect
International Journal of Heat and Mass Transfer 50 (2007) 208–215
International Journal of HEAT and MASS TRANSFER
www.elsevier.com/locate/ijhmt

Experimental investigation and modelling of heat transfer during convective boiling in a minichannel

H. Boye *, Y. Staate, J. Schmidt

Institute of Fluid Dynamics and Thermodynamics, Otto-von-Guericke Universität Magdeburg, Universitätsplatz 2, D-39106 Magdeburg, Germany

Received 31 January 2005; received in revised form 24 April 2006
Available online 18 September 2006

Abstract

Flow boiling heat transfer characteristics of water are experimentally studied in a circular minichannel with an inner diameter of 1500 μm. The fluid flows upwards and the test section, made of the nickel alloy Inconel 600, is directly electrically heated. Thus, the evaporation takes place under the defined boundary condition of constant heat flux. Mass fluxes between 50 and 100 kg/(m^2 s) and heat fluxes from 10 to 115 kW/m^2 at an inlet pressure of 3 bar are examined.

Infrared thermography is applied to measure the outer wall temperatures of the minichannel. This experimental method permits the identification of different boiling regions, boiling mechanisms and the determination of local heat transfer coefficients. Measurements are carried out in single-phase flow, subcooled and saturated boiling regions. The experimental heat transfer coefficients in the region of saturated boiling are compared with correlations available in literature and with a physically founded model developed for convective boiling.

Keywords: Flow boiling; Minichannel; Infrared thermography; Heat transfer; Boiling mechanism

1. Introduction

The investigation of heat transfer during forced flow boiling in mini and microchannels is traced back to the problem of the cooling of electronic circuits, as it was formulated in the 80's of the 20th century. This problem was generated by the development of highly integrated circuits with increasing power densities, for which the existing air cooling was not sufficient. The miniaturisation of flow channels, initiated by microelectronics, has opened further application fields today. One example is chemical reaction engineering, where many reactions take place in the gaseous phase, so that liquid educts have to be evaporated. If batches are small, danger of explosion exists and/or thermal decomposition due to high heating surface temperatures may occur, then the evaporation of the educts in minichannels is advantageous. Furthermore, the miniaturisation of channel dimensions permits to reduce the size of the devices, so that requirements of minimum construction volumes and large power-to-weight ratios can be met, like for example in mobile fuel cell systems.

For the design of these compact evaporators, generally accepted correlations are required to calculate the heat transfer coefficients and the pressure drop.

The equations available in literature are generally applicable to conventionally dimensioned channels. The question of the transferability of such two-phase flow heat transfer correlations to mini and microchannels is still under discussion. Kandlikar [1], Palm [2], Wadekar [3] and Celata [4] have made comprehensive reviews of relevant published studies of heat transfer in minichannels, e.g., Moriyama and Inoue [5], Cornwell and Kew [6], Oh et al. [7], Yan and Lin [8]. They obtained partially non-uniform trends of the heat transfer for flow boiling in mini and microchannels. In order to be able to design compact evaporators more precisely, further experimental investigations are necessary.

* Corresponding author. Tel.: +49 3916718576; fax: +49 3916712762.
E-mail address: hartwig.boye@vst.uni-magdeburg.de (H. Boye).

0017-9310/$ - see front matter © 2006 Elsevier Ltd. All rights reserved.
doi:10.1016/j.ijheatmasstransfer.2006.06.017

Nomenclature

c_p	specific heat capacity, J/(kg K)
d	diameter, m
I	electric current, A
L	length, m
$\dot{m}$	mass flux, kg/(m^2 s)
$\dot{M}$	mass flow rate, kg/s
p	pressure, Pa
$\dot{q}$	heat flux, W/m^2
$\dot{q}_V$	rate of energy generation per unit volume, W/m^3
r	radial coordinate, m
R	radius, m
R_{el}	electric resistance, Ω
s	slip, –
T	temperature, K
$\bar{T}_l$	caloric mean temperature of the fluid, K
u	axial velocity, m/s
$\bar{u}$	mean velocity, m/s
U	voltage, V
x	vapour quality, kg/kg
z	axial coordinate, m

Greek symbols

α	heat transfer coefficient, W/(m^2 K)
δ	film thickness, m
η	dynamic viscosity, N s/m^2
ϑ	temperature, °C
λ	heat conductivity, W/(m K)
ρ	density, kg/m^3
ρ_{el}	electrical resistivity, Ω m
σ	average error of heat transfer coefficient, W/(m^2 K)

Subscripts

in	inner
K	Kandlikar and Balasubramanian [15]
l	liquid
loss	loss
M	model
out	outer
ph	phase boundary
R	reference value
s	saturated
v	vapour
w	wall
Wa	VDI-Waermeatlas [14]
0	inlet

The present study focusses on investigating boiling heat transfer of water in a minichannel. In contrast to common experimental methods, the outer wall temperatures of the test section are measured without contact and axial profiles are obtained without time delay. This was done with a thermographic measuring method, which permits

- the study of the characteristic pulsative operation mode of a mini evaporator by continuous observation of the local channel wall temperatures,
- the quantitative demarcation of boiling ranges and precise characterisation of boiling mechanisms,
- the determination of axial heat transfer coefficients during two-phase flow.

This experimental procedure has already been successfully used by Hapke et al. [9,10] and provided useful information about boiling mechanisms in mini and microchannels.

The experimental heat transfer coefficients are compared with existing correlations for conventionally dimensioned channels. The registered qualitative and quantitative differences were the reason to generate a heat transfer model for convective boiling. In the case of water evaporation in the minichannel, this boiling mechanism exists over a relatively wide parameter range. The model is based on a slip model, which can be analytically formulated considering laminar flow for the vapour and liquid phases.

2. Experimental setup and data reduction

The test facility is schematically shown in Fig. 1. It is open to the atmosphere and consists of the basic components reservoir (1), dosing pump (2), mass flow meter (3), test section (4), condenser (5), power supply (6), infrared (IR) camera and traverse system unit (7) as well as data acquisition and evaluation system (8).

A hydrodynamically developed flow of subcooled water enters the test section with upward flow direction. The test section is a capillary tube made of Inconel 600 (nickel based alloy 2.4816) with an inner diameter of 1.5 mm, 500 mm length and a wall thickness of 0.75 mm. The channel is directly electrically heated, so that the evaporation experiments can be carried out approximately at the boundary condition $\dot{q} = \text{constant}$. Thereby the influence of the temperature-dependence of electrical resistivity $\rho_{el}(T)$ on this boundary condition can be neglected, since this resistivity value for Inconel 600 within the considered temperature range changes only about 2%. On the other hand, the heat losses to the environment by radiation and convection show a slight influence on the local value of $\dot{q}$. An advanced thermal insulation, like for instance a vacuum box, is not employed. Such an insulation, through which the heat losses due to convection can be completely eliminated, has to be transparent for the wavelengths corresponding to the long wave range of the camera (8–12 μm) and should be also extensively calibrated. In order

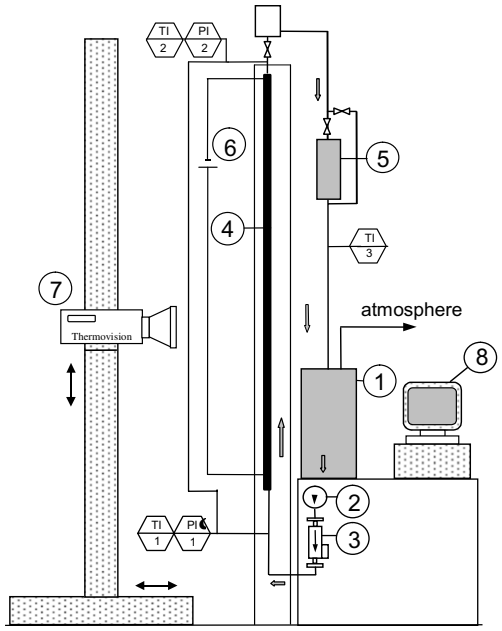

Fig. 1. Scheme of the test facility.

to avoid high calibration efforts, the given heat losses to the environment through convection and radiation are accepted. These heat losses $\dot{q}_{\text{loss}}$ depend on the operating conditions and are generally much lower than $\dot{q}$. The $\dot{q}_{\text{loss}}$ values are experimentally determined using a dry heated channel. Due to the different axial temperature distribution under both measurement and calibration conditions, the outer heat transfer coefficients differ slightly. These differences are negligible in the region of saturated boiling, where the wall temperature remains nearly constant.

The same dry heated channel is used also for the calibration of the surface emissivity. The outer surface is coated with a special thin black lacquer layer, which provides large values of emissivity. Since the exact heat conductivity resistance of the lacquer is not available, the calibration is referred to the metallic outer wall temperature, which can be calculated under inner adiabatic conditions.

The outer wall temperatures are scanned during the upward motion of the IR-camera (AGEMA THV 900), which is uniformly moved by the traverse system at a velocity of 15 mm/s. Since the scanning frequency is 15 frames per second, each axial position z is registered in 15 consecutive images over the time period of 1 s with a local resolution of 0.12 mm/pixel, see Fig. 2.

For the data evaluation, horizontal analysis lines are positioned on each picture, Fig. 2a. The maximum value of the temperature distribution on every analysis line is appraised as local wall temperature, Fig. 2b. Since the wall temperature is determined 15 times in 1 s at each axial location, a time averaged value of the temperature can be obtained. The averaged maximum temperatures are represented by $\bar{T}_{\text{w,out}} = f(z)$, Fig. 2c. The inner wall temperature $T_{\text{w,in}}(z)$ is calculated by using the solution of steady state heat conduction and is used for the determination of the local heat transfer coefficient, which is defined as follows

$$\alpha(z) = \frac{\dot{q}(z)}{T_{\text{w,in}}(z) - T_{\text{R}}(z)}. \tag{1}$$

The local heat flux in Eq. (1) is evaluated from the measured electrical input power taking into account the heat losses to the environment and neglecting the axial heat conduction in the wall, see Eq. (2).

$$\dot{q}(z) = \frac{U^2}{\pi d_{\text{in}} L R_{\text{el}}} - \frac{d_{\text{out}}}{d_{\text{in}}} \dot{q}_{\text{loss}}(z) \tag{2}$$

The inner wall temperature is calculated from Eq. (3) (neglecting ΔT through the lacquer layer):

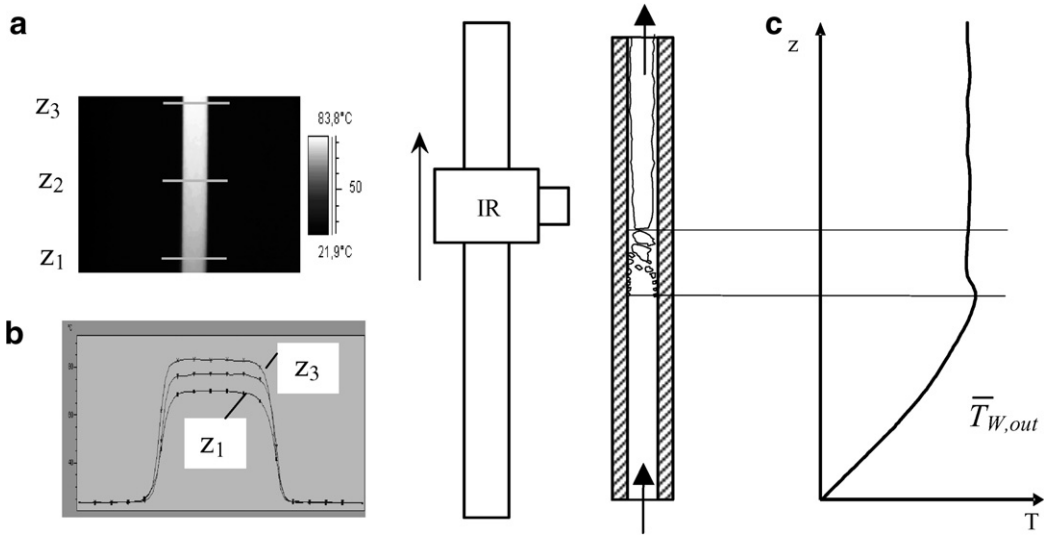

Fig. 2. Measurement and evaluation of the IR signals.

$$T_{w,in} = T_{w,out} + \frac{1}{2\lambda_w}\left[\frac{1}{2}\dot{q}_V\left(r_{out}^2 - r_{in}^2\right) - \left(\frac{UI}{\pi L} + \dot{q}_V r_{in}^2\right)\ln\left(\frac{r_{out}}{r_{in}}\right)\right] + \frac{r_{out}}{\lambda_w}\ln\left(\frac{r_{out}}{r_{in}}\right)\dot{q}_{loss}(T_{w,out}) \quad (3)$$

The caloric mean temperature of the fluid $\bar{T}_l$, Eq. (4),

$$\bar{T}_l(z) = T_0 + \frac{4}{\dot{m} d_{in} c_{p,l}}\int_{z_0}^{z}\dot{q}(z)\,dz \quad (4)$$

is used in the single-phase region as reference value T_R and the boiling temperature $T_s(p)$ is used in the saturated boiling region. The pressure drop $p(z)$ is calculated using the absolute pressure measured at point PI1, and the pressure difference measured between inlet PI1 and outlet PI2, see Fig. 1.

The error analysis is carried out using the error propagation law

$$\sigma = \left[\left(\frac{\partial\alpha}{\partial U}\right)^2\Delta U^2 + \left(\frac{\partial\alpha}{\partial T_{w,out}}\right)^2\Delta T_{w,out}^2 + \left(\frac{\partial\alpha}{\partial p}\right)^2\Delta p^2\right]^{1/2}, \quad (5)$$

where the essential dependencies of the heat transfer coefficient α on the measured values are included. The uncertainty in the electrical voltage measurement is 1%. The error in the outer wall temperature measurement caused by uncertainty in the emissivity of the wall is 1 K and the pressure measurement uncertainty, which influences the boiling temperature accuracy is 50 mbar.

The analysis of the experimental uncertainties leads to an average error in the heat transfer coefficient within the range of 10–30% depending on the working conditions. This relatively high value is mainly caused by the uncertainties in the measured wall temperatures. Although the absolute value of this error is low, it has a relatively large influence on the heat transfer coefficient because of the small temperature difference $T_{w,in}(z) - T_s(z)$.

In the following section a physically founded model for convective boiling in minichannels is introduced.

This boiling regime is characterised by increasing heat transfer coefficients with increasing vapour quality. This trend is observed in the experiments over a relatively wide range of quality (Section 4).

3. Model for convective boiling

The model is based on an annular flow model, Fig. 3, and a separation of liquid and vapour phases is supposed. The liquid flows at the heated wall and the vapour flows in the core of the fluid stream.

In contrast to conventionally dimensioned channels, where turbulent annular flow usually dominates, laminar annular flow appears much often in minichannels, because, at similar mass fluxes, the characteristic lengths are comparably lower. Therefore, laminar flow of both phases is assumed in the considered minichannel (Staate [11]). Under this assumption, a simplified description of the transport problem can be achieved. The transport phenomena are generally influenced by turbulence effects, particularly in the steam region, and by phase interface effects under boiling conditions. Therefore, the presented model should be understood as a step within the scope of a successive approximation to the real physical phenomena.

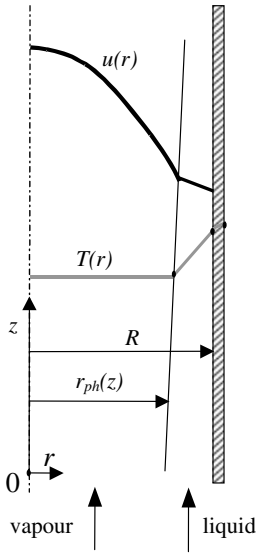

Fig. 3. Scheme of the two-phase flow in the convective boiling region.

In order to formulate an analytically solvable model, the following assumptions are made: steady state, incompressible flow of both phases, constant physical properties, neglection of the acceleration, mass and capillary forces as well as smooth interface, i.e., no waves at the phase boundary.

The flow model is derived using the momentum balances for the liquid and the vapour phases in form of Eqs. (6) and (7)

$$\frac{1}{r}\frac{d}{dr}\left(r\frac{du_l}{dr}\right) = \frac{1}{\eta_l}\frac{dp}{dz}, \quad (6)$$

$$\frac{1}{r}\frac{d}{dr}\left(r\frac{du_v}{dr}\right) = \frac{1}{\eta_v}\frac{dp}{dz}, \quad (7)$$

with the boundary conditions Eqs. (8)–(11)

$$\left.\frac{du_v}{dr}\right|_{r=0} = 0, \quad (8)$$

$$\eta_v\left.\frac{du_v}{dr}\right|_{r=r_{ph}} = \eta_l\left.\frac{du_l}{dr}\right|_{r=r_{ph}}, \quad (9)$$

$$u_v(r = r_{ph}) = u_l(r = r_{ph}), \quad (10)$$

$$u_l(r = R) = 0. \quad (11)$$

The solution of the equations system (6)–(11) results in local velocities of the liquid and vapour phases, Eqs. (12) and (13),

$$u_l(r,z) = \frac{1}{4\eta_l}\left|\frac{dp}{dz}\right| R^2\left[1-\left(\frac{r}{R}\right)^2\right], \tag{12}$$

$$u_v(r,z) = \frac{1}{4\eta_v}\left|\frac{dp}{dz}\right| R^2\left[\frac{\eta_v}{\eta_l}\left(1-\left(\frac{r_{ph}}{R}\right)^2\right)+\left(\frac{r_{ph}}{R}\right)^2-\left(\frac{r}{R}\right)^2\right], \tag{13}$$

from which the mean phase velocities can be determined

$$\bar{u}_l(z) = \frac{2}{R^2\left(1-\left(\frac{r_{ph}}{R}\right)^2\right)}\int_{r=r_{ph}}^{r=R} u_l(r,z)r\,dr = \frac{1}{8\eta_l}\left|\frac{dp}{dz}\right| R^2\left[1-\left(\frac{r_{ph}}{R}\right)^2\right], \tag{14}$$

$$\bar{u}_v(z) = \frac{2}{r_{ph}^2}\int_{r=0}^{r=r_{ph}} u_v(r,z)r\,dr = \frac{1}{8\eta_v}\left|\frac{dp}{dz}\right| R^2\left[2\frac{\eta_v}{\eta_l}\left(1-\left(\frac{r_{ph}}{R}\right)^2\right)+\left(\frac{r_{ph}}{R}\right)^2\right]. \tag{15}$$

After the elimination of axial pressure gradients in Eqs. (14) and (15), the obtained equation is used for the substitution of the mean liquid velocity in the global mass balance, Eq. (16),

$$\dot{M} = \bar{u}_v \pi r_{ph}^2 \rho_v + \bar{u}_l \pi\left(R^2 - r_{ph}^2\right)\rho_l = u_{l,0}\pi R^2 \rho_{l,0}, \tag{16}$$

so that an equation for the mean vapour velocity can be achieved and where $r_{ph}^* = r_{ph}/R$ is introduced:

$$\bar{u}_v(z) = \frac{\bar{u}_{l,0}(z)\frac{1}{r_{ph}^{*2}}\frac{\rho_{l,0}}{\rho_v}}{1+\frac{\rho_l}{\rho_v}\frac{\eta_v}{\eta_l}\frac{1}{r_{ph}^{*4}}\frac{\left(1-r_{ph}^{*2}\right)^2}{1+2\frac{\eta_v}{\eta_l}\frac{1-r_{ph}^{*2}}{r_{ph}^{*2}}}}. \tag{17}$$

After the introduction of Eq. (17) in the quality equation, Eq. (18),

$$x = \frac{\dot{M}_v}{\dot{M}} = \frac{\bar{u}_v(z)\pi r_{ph}^2 \rho_v}{\bar{u}_{l,0}\pi R^2 \rho_{l,0}}, \tag{18}$$

Eq. (19) can be deduced

$$\frac{\rho_l}{\rho_v}\frac{\eta_v}{\eta_l}\frac{x}{1-x} = \frac{\left(\frac{r_{ph}}{R}\right)^4 + 2\frac{\eta_v}{\eta_l}\left(\frac{r_{ph}}{R}\right)^2\left(1-\left(\frac{r_{ph}}{R}\right)^2\right)}{\left(1-\left(\frac{r_{ph}}{R}\right)^2\right)^2} \tag{19}$$

and simplified by neglecting the second term in the numerator [11]

$$\sqrt{\frac{\rho_l}{\rho_v}\frac{\eta_v}{\eta_l}\frac{x}{1-x}} = \frac{\left(\frac{r_{ph}}{R}\right)^2}{1-\left(\frac{r_{ph}}{R}\right)^2}. \tag{20}$$

Using the solution of Eq. (20), the phase interface radius $r_{ph}\left(R, x(z), \frac{\eta_v}{\eta_l}, \frac{\rho_l}{\rho_v}\right)$ can be determined and so the axially changing liquid film thickness $\delta = R - r_{ph} = \delta\left(R, x(z), \frac{\eta_v}{\eta_l}, \frac{\rho_l}{\rho_v}\right)$.

Furthermore, with Eqs. (14) and (15), the so-called slip of the two-phase flow can be achieved:

$$s = \frac{\bar{u}_v(z)}{\bar{u}_l(z)} = 2 + \frac{\eta_l}{\eta_v}\frac{\left(\frac{r_{ph}}{R}\right)^2}{1-\left(\frac{r_{ph}}{R}\right)^2} \tag{21}$$

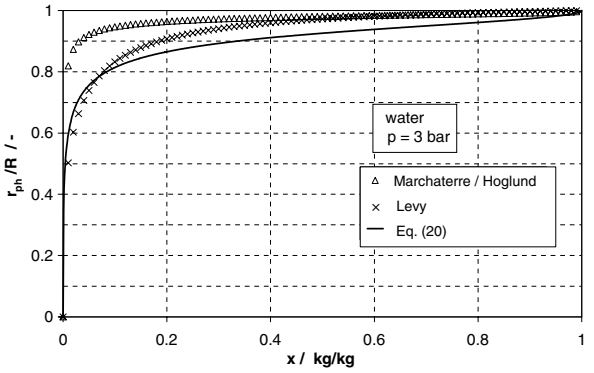

Fig. 4. Phase interface radius vs. quality.

In Fig. 4, the phase interface radius is shown over quality for water.

The phase interface radius increases with increasing quality and thus, the liquid film thickness decreases. Considerably smaller values of the liquid film thickness over a wide range of quality are obtained using the slip models of Levy [12], Marchaterre and Hoglund [13].

The knowledge of the axial dependence of the phase interface radius, according to Eq. (20), makes it possible to determine the heat transfer coefficient on the basis of a film model. This model assumes that the heat transfer takes place only by radial heat conduction through the liquid layer, which is considered to be smooth and planar. Then, the heat transfer coefficient can be obtained:

$$\alpha_M(z) = \frac{\lambda_l}{R - r_{ph}(z)} = \frac{\lambda_l}{\delta(z)}. \tag{22}$$

In Fig. 5, the model heat transfer coefficients are given over quality and compared with values resulting from the slip models of Levy, Marchaterre and Hoglund by using the film model.

The model heat transfer coefficient increases with increasing quality due to the decrease of the liquid film thickness. As mentioned, film waviness, which would increase the heat transfer coefficient, is not considered in this model.

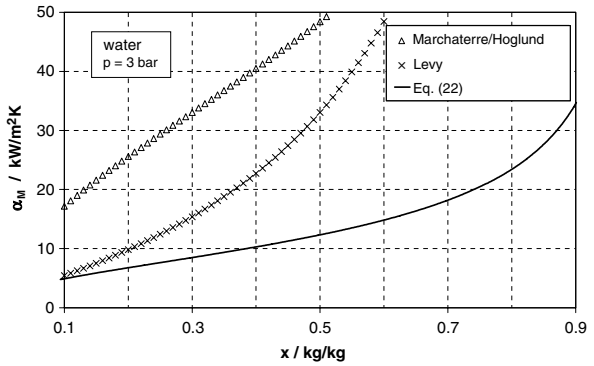

Fig. 5. Model heat transfer coefficients vs. quality.

Because of the smaller liquid film thicknesses, the heat transfer coefficients calculated from the models of Levy, Marchaterre and Hoglund are considerably higher than the results from our own model over a wide range of qualities.

In the following section, the experimental results are compared with those obtained using the theoretical model.

4. Results

Series of experiments are carried out by varying heat and mass flux under the defined boundary condition $\dot{q} = \text{constant}$. The operating pressure is 3 bar and the working fluid, water, enters the test section at ambient temperature of about 30 °C.

In the following, exemplary measurement results of the axial wall temperatures, which are used for the determination of the axial heat transfer coefficient, are shown as a function of the heat flux, Fig. 6.

In Fig. 7, the heat transfer coefficients vs. length z are given for the heat flux $\dot{q} = 94.7\ \text{kW/m}^2$. The wall and the fluid temperatures are also shown.

In the single-phase flow region, up to a length of $z = 0.085$ m, the heat transfer coefficient is influenced by the thermal entrance and by the effect of the axially dependent heat losses.

The heat transfer coefficient increases while approaching the onset of boiling and achieves a relative maximum within the subcooled boiling region. After a significant drop of the heat transfer coefficient, which is typical for the obtained experimental results, the heat transfer coefficient increases over a relatively wide length range. It is assumed that this increase is caused by the mechanism of convective boiling. The values of the presented film model (Eq. (22)) show a satisfying qualitative and quantitative agreement with the measured coefficients in the medium quality region.

The drop of the heat transfer coefficients near the channel exit is assumed to be caused not by the boiling process but by the thermographic measuring effects, mainly due to the reflections of the radiation coming from the electrical connection of the power supply.

The comparison between the measured values and correlations available in literature (VDI-Waermeatlas [14], Kandlikar and Balasubramanian [15]) yields only a qualitative agreement. The calculated correlation values show the same trend of increasing heat transfer coefficients which is characteristic for the mechanism of convective boiling. However, there are considerable quantitative differences. The literature-supported values, which are obtained by extrapolation of the correlations to the given characteristic length ($2R$), are 2–3 times larger in some regions than the experimental data.

These differences can be explained in the case of the VDI-Waermeatlas correlation, which is based on the measured values for channels with characteristic lengths higher than 4 mm. Turbulence and boundary surface effects (waviness) can lead to higher heat transfer coefficients within the region of convective boiling in conventionally dimensioned channels than in the investigated minichannel, in which laminar flow conditions are often given for the liquid phase.

The experimental results with variation of the heat flux are shown in Fig. 8. Due to the typically small differences between wall and fluid temperature, little uncertainties in

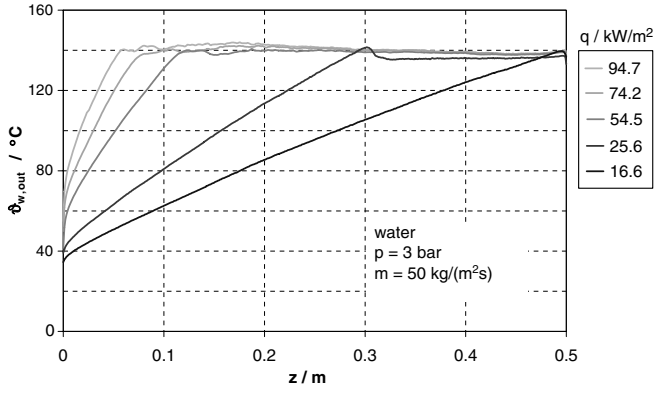

Fig. 6. Axial wall temperatures for various heat fluxes, $\dot{m} = 50\ \text{kg/(m}^2\text{s)}$.

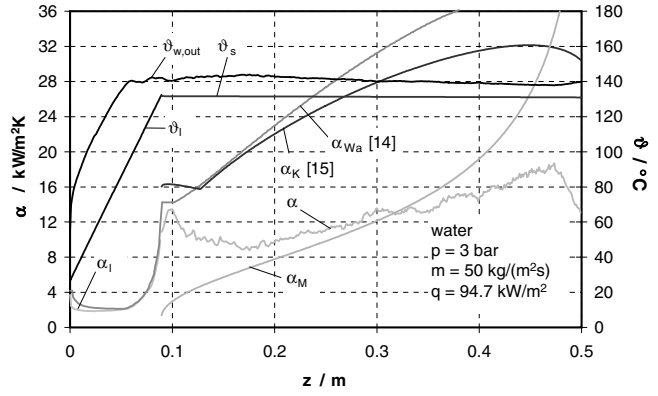

Fig. 7. Temperatures and heat transfer coefficients.

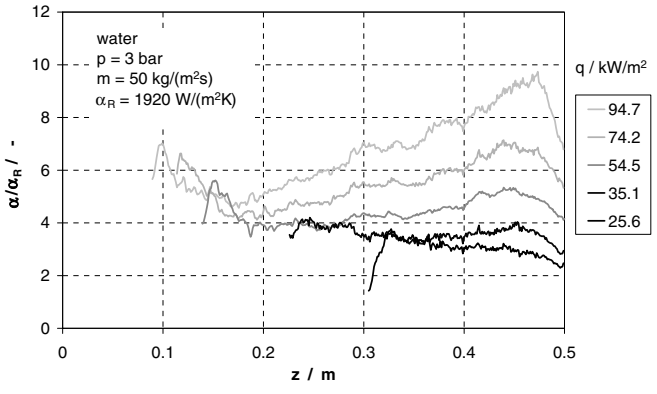

Fig. 8. Scaled local heat transfer coefficients for various heat fluxes, $\dot{m} = 50\ \text{kg/(m}^2\text{s)}$.

the temperature measurement have, as mentioned before, a strong influence on the accuracy of the experimental heat transfer coefficients. Therefore, a suitably scaled heat transfer coefficient is introduced in Fig. 8. The axial distribution of this scaled heat transfer coefficient describes precisely the characteristic trends caused by the different boiling mechanisms.

The scaled heat transfer coefficient is defined by using the single-phase heat transfer coefficient α_R immediately before the onset of boiling, where the wall temperature of the test section agrees approximately with the wall temperatures in the flow boiling region.

It is assumed that the experimental uncertainty of this reference value α_R caused by the thermographic wall temperature measurement as well as by the measurement of $\dot{q}$ and $\dot{m}$ agrees with the corresponding measurement error of the flow boiling heat transfer coefficient. Thus, it is expected that, during the dividing of the heat transfer coefficient α by the reference value α_R, the uncertainty of the scaled heat transfer coefficient α/α_R will be generally reduced.

The plots in Fig. 8 show that convective boiling clearly dominates at larger heat fluxes. Thereby, it should be noted that the range of decreasing heat transfer coefficients after the onset of boiling is still not complete at the lowest heat flux.

The experimental results can be generalised by plotting the scaled heat transfer coefficients over the quality. According to the model given in Eq. (22), beside the physical properties $\lambda_l, \eta_l/\eta_v, \rho_l/\rho_v$ and the characteristic length $2R$ of the channel, the heat transfer coefficient for convective boiling depends mainly on the quality. This dependence can be clearly observed in Fig. 9, where the literature-supported values for $\dot{q} = 94.7\ \mathrm{kW/m^2}$ are shown for comparison.

Unlike the chart in Fig. 8, which represents the heat transfer coefficients over the channel length z, the plots α/α_R vs. x coincide in Fig. 9. However, a certain dependence on the heat flux, which is not described by the model, Eq. (22), is obtained. The theoretical function $\alpha_M/\alpha_R = f(x)$

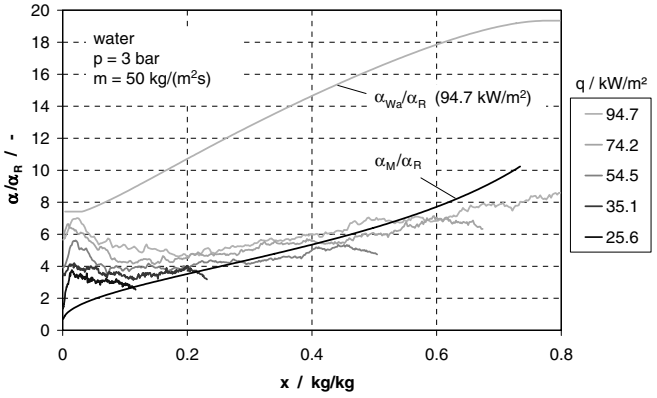

Fig. 9. Scaled local heat transfer coefficients vs. quality for various heat fluxes, $\dot{m} = 50\ \mathrm{kg/(m^2\,s)}$.

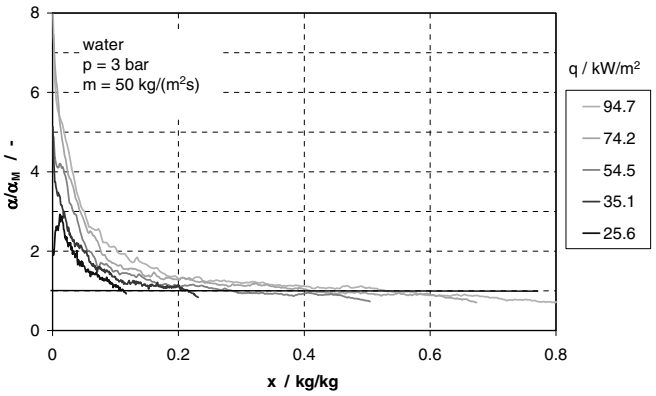

Fig. 10. Local heat transfer coefficients scaled by the model values vs. quality for various heat fluxes, $\dot{m} = 50\ \mathrm{kg/(m^2\,s)}$.

is, in particular at medium x-values, in satisfying agreement with the experimental values. As a consequence of this, all experimental profiles in a plot of $\alpha/\alpha_M = f(x)$, Fig. 10, approximate to one.

The curves in Fig. 10 have hyperbolic characteristics and constitute the basis for the formulation of an empirical correlation, which can be described by Eq. (23)

$$\frac{\alpha}{\alpha_M} = A + \frac{B}{x + C}. \tag{23}$$

The coefficients A and C show no clear dependence on the heat flux. Their average values amount $A = 0.57$ and $C = 0.027$. The dependence of the function $\alpha/\alpha_M = f(x, \dot{q})$ on the heat flux will be taken into account by the B coefficient, see Fig. 11, which can be described by the numerical-value Eq. (24):

$$B(\dot{q}) = 0.0015\dot{q} + 0.05 \quad \dot{q}/\mathrm{kW/m^2}. \tag{24}$$

The correlations (23) and (24) will be applied for the dimensioning of compact evaporators. The results will be presented in a following paper. Since the correlations are valid only under the given experimental conditions in the medium quality region, their application to the dimensioning of compact evaporators should have the character of a rough estimation and can be understood as a step in the

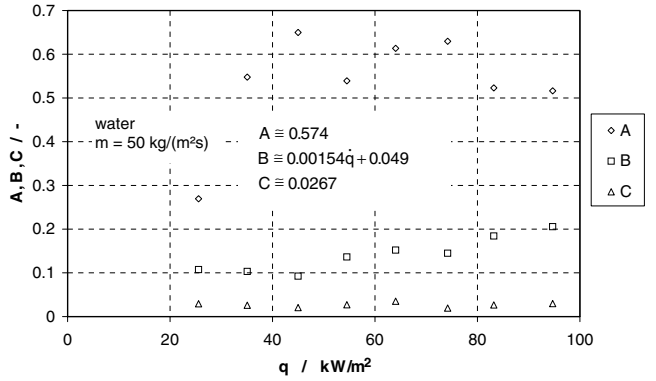

Fig. 11. Coefficients A, B and C from Eq. (23) vs. heat flux.

successive approximation to the corresponding compact evaporator dimensioning algorithms.

5. Conclusions

Experimental investigations on flow boiling in a minichannel are conducted. Water is used as working fluid. The directly electrically heated test section is a circular tube with an inner diameter of 1500 μm. Experimental results are presented up to a quality of 0.8 for a mass flux of 50 kg/(m^2s) and heat fluxes from 15 to 100 kW/m^2 at an inlet pressure of about 3 bar.

The applied thermographic measuring method provides transient and axial profiles of the wall temperature.

In principle, two boiling mechanisms are observed. A characteristic nucleate boiling takes place in the subcooled region with a relative maximum of the heat transfer coefficient distribution. Afterwards, the heat transfer coefficients increase over a wide range of quality and are relatively weak dependent on the heat flux. This indicates convective boiling, whose analysis is regarded to be the main focus of this paper.

In comparison with some correlations selected from the literature, the own experimental heat transfer coefficients are clearly smaller within the region of convective boiling. This can be attributed to the laminar character of the annular flow assumed in the investigated minichannel in comparison to the generally dominating turbulent flow of both phases in conventionally dimensioned channels.

The assumed annular flow in the minichannel is the basis for the formulation of an analytically solvable two-fluid model for the convective boiling region. In consideration of the momentum and mass balances of both phases, a slip model is derived for the determination of the liquid film thickness. The theoretical heat transfer coefficients are obtained using a film model. The experimental heat transfer coefficients agree satisfactorily with the model values in the medium quality region.

The scaling of the experimental heat transfer coefficient using the model heat transfer coefficient enables the formulation of an analytic function of the heat transfer coefficient against quality and heat flux. This analytic function will be implemented in a dimensioning program for compact evaporators.

References

[1] S.G. Kandlikar, Two-phase flow patterns, pressure drop, and heat transfer during boiling in minichannel flow passages of compact evaporators, Heat Transfer Eng. 23 (2002) 5–23.
[2] B. Palm, Heat Transfer in Microchannels, in: Proceedings of the International Conference on Heat Transfer and Transport Phenomena in Microscale, Banff, Canada, 2000, pp. 54–65.
[3] V.V. Wadekar, Compact heat exchangers for phase change, Int. J. Heat Exch. 3 (2002) 169–200.
[4] G.P. Celata, Heat Transfer and Fluid Flow in Microchannels, in: G.F. Hewitt (Ed.), Series in Thermal and Fluid Physics and Engineering, Begell House, Inc., 2004.
[5] K. Moriyama, A. Inoue, The thermohydraulic characteristics of two-phase flow in extremely narrow channels, Heat Transfer – Jpn. Res. 21 (8) (1992) 838–856.
[6] K. Cornwell, P.A. Kew, Evaporation in microchannel heat exchangers, IMechE, C510/117/95, (1995) 289–293.
[7] H. Oh, M. Katsuta, K. Shibata, Heat transfer characteristics von R134a in a capillary tube heat exchanger, Heat Transfer 1998, in: Proceedings of the 11th IHTC, Kyongju, Korea, vol. 6, 1998, pp. 131–136.
[8] Y.Y. Yan, T.F. Lin, Evaporation heat transfer and pressure drop of refrigerant R134a in a small pipe, Int. J. Heat Mass Transfer 41 (1998) 4183–4194.
[9] I. Hapke, H. Boye, J. Schmidt, Onset of Nucleate Boiling in Minichannels, Int. J. Therm. Sci. – Revue Generale de Thermique 39 (2000) 505–513.
[10] I. Hapke, H. Boye, J. Schmidt, Flow Boiling of Water and *n*-Heptane in Microchannels, Microscale Thermophys. Eng. 6 (2002) 99–115.
[11] Y. Staate, Wärmeübergang beim Strömungssieden im Minikanal, Dissertation, Magdeburg, 2004.
[12] S. Levy, Steam-slip – theoretical prediction from momentum model, Trans. ASME, Ser. C, J. Heat Transfer 82 (1960) 113–124.
[13] J.F. Marchaterre, B.M. Hoglund, Correlation for two-phase flow, Nucleonics 20 (1962) 142.
[14] VDI-Waermeatlas, Springer-Verlag, Berlin, 2002.
[15] S.G. Kandlikar, P. Balasubramanian, Extending the applicability of the flow boiling correlation to low Reynolds number flows in microchannels, in: first International Conference on Microchannels and Minichannels; April 24–25, Rochester, New York, USA; ICMM2003-1075, 2003.